Contents lists available at ScienceDirect

Materials Chemistry and Physics

journal homepage: http://ees.elsevier.com

Synthesis of SiOC using solvent-modified polymer precursors

Donald Erb, Kathy Lu*

Department of Materials Science and Engineering, Virginia Polytechnic Institute and State University, Blacksburg, VA, 24061, USA

ARTICLE INFO

Keywords
Silicon oxycarbide
3-pentanone
n-heptane
isobutylbenzene
SiC formation

ABSTRACT

Silicon oxycarbide ceramics are an important class of materials that can be modified to cover a wide range of microstructures and compositions during processing. This study focuses on a polysiloxane precursor to SiOC conversion when crosslinked in the presence of 0, 50, 100, and 200 vol% of 3-pentanone, n-heptane, or isobutylbenzene, relative to the volume of the polysiloxane. The solvent modified samples show a decrease in bulk density and an increase in open porosity. The addition of the solvents facilitates the formation of crystalline SiC, especially for 3-pentanone. The ability of the solvents to encourage SiC formation is directly related to the solvent molecular size, with smaller solvents being more likely to increase polymer chain entanglement and remain trapped within the polymer after drying and subsequently creating more C-C and Si-C bonds after pyrolysis. This work shows the unique function of solvents in modifying the SiOC microstructures and properties.

1. Introduction

Silicon oxycarbide (SiOC) is an amorphous ceramic, consisting of SiO_xC_{4-x} bonds, where $0 < x < 4$, and free carbon when pyrolyzed at temperatures lower than ~1250 °C. At ≥1300 °C pyrolysis temperatures, an amorphous/nanocrystalline composite forms. Due to SiOC being a polymer derived ceramic, its properties and compositions are highly configurable simply by controlling the chemistry of the preceramic polymer(s) and the processing conditions. SiOC has a wide range of tailorable properties, such as porosity, high temperature stability, oxidation resistance, and electrical conductivity [1–3]. Porous SiOC has gained much attention for applications such as electrodes in lithium ion batteries, catalyst supports, gas separation membranes, lightweight components, and thermal barriers [4–6]. Likewise, dense SiOC is promising in applications such as coatings and structural components due to its resistance to oxidation/crystallization at elevated temperatures and excellent mechanical properties [1,7,8].

Solvents have been widely used during gelation in the fabrication of silica gels [9]. After gelation, the solvent is removed either by supercritical drying, most often using supercritical CO_2, or through subcritical drying, such as drying at ambient temperature and pressure [6,9–12]. For polymer derived ceramics, porosity can be introduced through the use of a solvent during crosslinking followed by removal of the solvent by drying. The selection of the solvent and solvent concentration has significant effects on the drying behavior, pore size, and pore morphology of both the polymer and the SiOC after pyrolysis [12–15]. Sasikumar et al. [12] crosslinked polyhydromethylsiloxane and divinylbenzene in the presence of either acetone or cyclohexane as a solvent, followed by CO_2 supercritical drying. After pyrolysis in argon, the sample crosslinked in acetone had a specific surface area of 215 m^2/g and a pore volume of 0.87 m^3/g, while the sample crosslinked in cyclohexane had a specific surface area of 108 m^2/g and a pore volume of 0.20 m^3/g. Furthermore, the pore size of the acetone sample was between 20 and 30 nm, while the pore size of the cyclohexane sample was much smaller, around 4 nm. It should also be pointed out that the porosity introduced during crosslinking or the early stages of pyrolysis is transient and usually disappears at temperatures greater than 600–800 °C [16,17].

Although the use of various solvents to alter the polymer pore structure before pyrolysis has been investigated, the effect of solvents on the thermophysical properties, structural evolution, and microstructure of SiOC has not been carefully studied. Tamayo et al. [13] investigated the effect of aging polydimethylsiloxane (PDMS) and tetraethyl orthosilicate (TEOS) hybrid gels in acetone, isopropanol, and n-hexane on the properties of the obtained SiOC after pyrolysis. It was claimed that polar solvents, such as acetone and isopropanol, more easily remove non-bonded PDMS molecules from the gel [13,15]. With increasing aging time, the polar solvents decreased the carbon crystallite sizes within the SiOC after pyrolysis at 1100 °C while the non-polar solvent showed the opposite trend [13]. For the SiOC synthesized using polyhydromethylsiloxane and divinylbenzene and crosslinked in the presence of either acetone or cyclohexane, the sample crosslinked in acetone had a slightly smaller carbon domain size compared to the non-polar cyclohexane after pyrolysis at 900 °C [12]. Since the properties of SiOC,

* Corresponding author.
Email address: klu@vt.edu (K. Lu)

https://doi.org/10.1016/j.matchemphys.2019.121844
Received 8 June 2018; Received in revised form 9 June 2019; Accepted 9 July 2019
Available online xxx
0254-0584/

such as its stability in air, are heavily dependent on its chemical and phase compositions, further understanding of the solvent effects is needed.

In this work, SiOC ceramics are fabricated after pyrolysis of a polysiloxane crosslinked in the presence of three different solvents: 3-pentanone, n-heptane, or isobutylbenzene. The effects of different solvents and the amount of solvents on the resulting thermophysical properties, phase evolution, and microstructure of the SiOC ceramics are studied.

2. Experimental procedures

A commercial polysiloxane (PSO, $[\text{-Si}(C_5H_6)_2\text{O-}]_3[\text{-Si}(CH_3)(H)\text{O-}]_2[\text{-Si}(CH_3)(CH=CH_2)\text{O-}]_2$, SPR-684, Starfire Systems, Inc., Gelest Inc., Schenectady, NY) was chosen as the base precursor and 2.1–2.4% platinum-divinyltetramethyldisiloxane complex in xylene (Pt catalyst, Gelest Inc., Morrisville, PA) was used as the catalyst. The three solvents used were 3-pentanone (Fisher Scientific, Pittsburgh, PA), n-heptane (Fisher Scientific, Pittsburgh, PA), and isobutylbenzene (Fisher Scientific, Pittsburgh, PA). The chemical structures of the three solvents are shown in Fig. 1.

First, solutions with PSO and either 0, 50, 100, or 200 vol% solvent (relative to the PSO volume) were sonicated for 10 min and then mixed in a high energy mill (SPEX 8000 M Mixer/Mill, SPEX SamplePrep, Metuchen, NJ) for 10 min to form a homogeneous mixture. Next, the Pt catalyst (1 wt% relative to PSO) was added, the mixtures were mixed again in a high energy ball mill for 5 min, and then poured into aluminum foil molds. The mixtures were placed into a vacuum chamber and vacuumed for 10 min at 200 Torr to remove any bubbles in the solutions. The molds were then sealed in acid digestion vessels to prevent evaporation of the solvents and placed in an oven to crosslink at 50 °C for 12 h and then at 120 °C for 6 h. After crosslinking, the molds were removed from the acid digestion vessels and dried at room temperature for 24 h, 50 °C for 12 h, and 120 °C for 6 h to remove all the solvent. The samples designated as PSO corresponded to the pure PSO composition; the samples with solvent additions were labelled as X-p, X-h, and X-i, where h, p, and i correspond to 3-pentanone, n-heptane, and isobutylbenzene, respectively, and X was the volume percent of solvent (50, 100, or 200).

To prepare the samples for pyrolysis, the crosslinked specimens were cut and polished into square pieces roughly 10 mm in length and 2 mm in thickness. Next, the samples were placed into a zirconia crucible, covered on both sides with graphite mats in order to reduce friction during shrinkage and prevent warping [18,19], and put into a tube furnace (1730-20 Horizontal Tube Furnace, CM Furnaces Inc., Bloomfield, NJ). With an Ar flow rate of about 500 std cm^3/min, the samples were heated up to 1300 °C at a rate of 1 °C/min, held for 2 h, cooled to 400 °C with a rate of 1 °C/min, and finally cooled to 50 °C with a rate of 2 °C/min. During heating from 500°C to 700 °C, the Ar gas flow was bubbled through water at 60 °C, giving a gas flow with a Ar:H_2O molar ratio of approximately 5:1; the water vapor injection encouraged SiO_2 formation within the SiOC, but was not the focus of this study [20,21].

Ceramic yield was calculated by measuring the mass of the samples before and after the pyrolysis. The bulk density and porosity of the resulting SiOCs were measured using the Archimedes method with ethanol as the saturating and submersion medium. The chemical bonding of the polymers was evaluated using Fourier Transform Infrared Spectroscopy (FT-IR) (Nicolet 8700 with Pike GladiATR attachment, Thermo Scientific, Waltham, MA), which recorded light absorbance between 500 and 4000 cm^{-1} wavenumber with a resolution of 4 cm^{-1} and averaged between 64 scans. The decomposition behavior of the polymer samples was measured using thermogravimetric analysis (TGA) (Q50, TA Instruments, New Castle, DE) with a heating rate of 2 °C/min and an argon flow of 40 mL/min. The specific surface area and pore volume of micro-/meso-pores within the bulk samples after pyrolysis were measured using nitrogen adsorption at 77 K (NOVA 2200e, Quantachrome Instruments, Boynton Beach, FL). The phase compositions of the pyrolyzed samples were analyzed in an X'Pert PRO diffractometer (PANalytical B.V., EA Almelo, the Netherlands) with Cu Kα radiation. A field emission SEM (LEO 1550, Carl Zeiss MicroImaging, Inc, Thornwood, NY) was used to characterize the microstructures of the pyrolyzed samples.

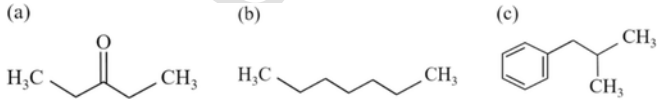

Fig. 1. Molecular structures of (**a**) 3-pentanone, (**b**) n-heptane, and (**c**) isobutylbenzene.

3. Results and discussion

3.1. Thermophysical properties

The ceramic yield values for the pyrolyzed samples are shown in Table 1. For all the pyrolyzed samples, the ceramic yields range from 67% to 72%. The addition of the solvents makes insignificant difference. In general, the ceramic yield increases slightly with the solvent content.

The open porosity of the SiOC samples after pyrolysis at 1300 °C ranges from 4.4 vol% – 14.3 vol%. The addition of the solvents increases the open porosity of the SiOC samples relative to the pure PSO sample. For 3-pentanone, the porosity decreases from 9.5 vol% for the 50-p sample to 4.4 vol% for the 200-p sample. For the n-heptane samples, the open porosity increases from 7.9 vol% for the 50-h sample to 14.3 vol% for the 200-h sample. The porosity for the isobutylbenzene samples decreases from 8.8 vol% for the 50-i sample to 7.9 vol% for the 200-i sample. The faster drying of the polymer in this study may have contributed to the lack of a significant amount of porosity compared to those in literature. For example, Aravind et al. [22] sealed the gel using aluminum foil and let it sit for two weeks before making a hole in the aluminum foil seal and further drying for one week at 50 °C. Further, there was a lack of micro- and meso-porosity within the samples as measured by nitrogen adsorption (0.001 cm^3/g for 200-p, 0.003 cm^3/g for 200-h, and 0.001 cm^3/g for 200-i) due to pore collapse during the aggressive drying.

The decrease in the open porosity with increasing solvent concentration for 3-pentanone and isobutylbenzene can be understood as follows. For low solvent concentrations, the PSO-solvent system is composed of the PSO polymer matrix with solvent molecules within the matrix. During drying, the system does not experience significant shrinkage due to the low solvent amount. For the higher solvent concentrations, the roles are reversed, with the PSO polymer within the

Table 1
Ceramic yield, open porosity, and bulk density of the SiOC samples after pyrolysis at 1300 °C.

Sample	Ceramic Yield (%)	Open Porosity (%)	Bulk Density (g/cm^3)
PSO	69.38 ± 1.12	6.0 ± 2.3	1.76 ± 0.01
50-p	69.31 ± 0.64	9.5 ± 4.1	1.61 ± 0.01
100-p	69.05 ± 0.49	6.5 ± 2.0	1.67 ± 0.07
200-p	70.25 ± 0.62	4.4 ± 0.5	1.69 ± 0.06
50-h	70.25 ± 1.55	7.9 ± 2.4	1.72 ± 0.02
100-h	70.29 ± 1.04	11.2 ± 2.6	1.65 ± 0.02
200-h	72.35 ± 0.85	14.3 ± 1.6	1.53 ± 0.02
50-i	67.16 ± 0.50	8.8 ± 5.0	1.70 ± 0.07
100-i	69.62 ± 0.39	8.7 ± 1.1	1.54 ± 0.07
200-i	69.63 ± 0.38	7.9 ± 1.5	1.71 ± 0.01

solvent solution; drying then removes a more significant amount of solvent and causes the polymer to collapse and pores to close. The decrease in open porosity for the samples with 3-pentanone and isobutylbenzene compared to the increase in open porosity for the samples in n-heptane may be due to the differences in the solvent surface tension. During drying, the pores experience a capillary pressure P, which depends on the solvent surface tension γ, pore radius r, and contact angle θ as [9]:

$$P = 2\gamma \frac{cos(\theta)}{r} \quad (1)$$

The surface tensions of the three solvents are 24.7 mN/m, 19.7 mN/m, and 28.8 mN/m for 3-pentanone, n-heptane, and isobutylbenzene, respectively [23]. Thus, with the same pore radius, 3-pentanone and isobutylbenzene would exert more capillary pressure on a pore during drying, due to their higher surface tensions, leading to more pore closure, less porosity in the polymer, and thus less porosity after pyrolysis.

The bulk density of the samples after pyrolysis ranges from 1.53 g/cm^3 – 1.76 g/cm^3. For all conditions, the addition of the solvents decreases the bulk density of the SiOC samples relative to the pure PSO sample. However, the bulk density trends are somewhat convoluted due to some residual closed pores and the differing amounts of SiC in the samples (Section 3.2). For the n-heptane samples, the density decreases from 1.72 g/cm^3 for the 50-h sample to 1.53 g/cm^3 for the 200-h sample. For the 3-pentanone samples, the density slightly increases from 1.61 g/cm^3 for the 50-p sample to 1.69 g/cm^3 for the 200-p sample. However, the density of the isobutylbenzene samples shows no trend and varies between 1.70 g/cm^3 for the 50-i sample, 1.54 g/cm^3 for the 100-i sample, and 1.71 g/cm^3 for the 200-i sample.

3.2. Structural evolution

The FT-IR spectra of the crosslinked polymers with the solvents after drying are compared to that of the PSO sample to determine whether the solvent presence during crosslinking affects the chemical bonding or crosslinking behavior of the polymer. Fig. 2(a) shows the FT-IR spectra of the pure PSO sample and the 200 vol% condition for each of the three solvents. All the samples show sharp peaks at ~695, 715, 740, 1130, and 1426 cm^{-1} wavenumber, which are characteristic of the phenyl side group in the base PSO. The peak at 1260 cm^{-1} wavenumber corresponds to the methyl side group, and a broad peak between 1000 and 1100 cm^{-1} wavenumber can be assigned to Si-O-Si [24]. The samples crosslinked with the different solvents show no major differences in their FT-IR spectra, which is to be expected since the solvents should not participate in the crosslinking. Fig. 2(b) shows the FT-IR spectra for the PSO polymer and the 50, 100, and 200 vol% 3-pentanone polymers. Similar to Fig. 2(a), there are no significant changes compared to the PSO sample when increasing the solvent content, signifying again that there is no detectable influence from the solvent on the polymer bonding.

For linear polysiloxanes, thermal decomposition first begins at temperatures ~350 °C due to depolymerization of the siloxane chain forming volatile cyclic siloxane species [25,26]. Thus, any significant mass loss before 350 °C can be attributed to residual solvent trapped within the polymer after drying. From the dTG curves in Fig. 2(c), all the 200 vol% solvent samples display a slight mass loss between 50 °C–300 °C, up to ~ 3%, consistent with another study [27]. Thus, although the residual solvent could not be detected using FT-IR, the TGA results show that there is a small concentration of solvents remaining in the polymers after drying. Also, 3-pentanone has the most delayed and least mass loss and mass loss rate than the other samples, meaning that it is the most effectively trapped within the dried polymer.

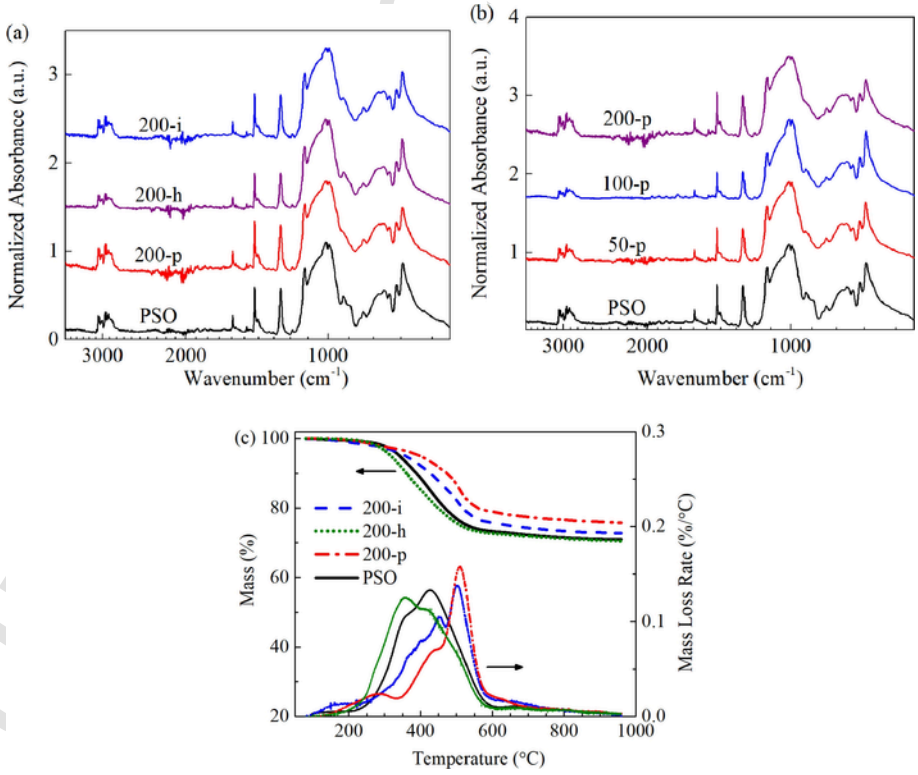

Fig. 2. FT-IR spectra for the polymer precursors after crosslinking. (**a**) 200 vol% solvents, and (**b**) three solvent amounts for 3-pentanone. (c) TGA and dTG of the 200 vol% solvent samples.

More significantly, n-heptane decreases the overall thermal stability of the PSO, causing a mode peak in the dTG at ~350 °C rather than at ~450 °C for the pure PSO, while 3-pentanone increases the thermal stability of the PSO polymer, delaying the dTG peak mode to >500 °C. Typically, an increase in the thermal stability of linear polymers with the same side groups can be attributed to an increase in the crosslinking density, due to either chemical bonds or physical entanglements [28,29]. Given that the solvents do not appreciably change the chemical bonding within the polymers, apparent from the FT-IR curves in Fig. 2(a) and (b), the increased thermal stability produced by 3-pentanone (especially considering its small size), and to a less extent isobutylbenzene, is due to the solvents encouraging physical entanglements during crosslinking. In addition, in Fig. 2(c), the 3-pentanone sample has the least mass loss during the entire thermal analysis range, meaning that the solvent extends its impact into the final pyrolyzed samples. Isobutylbenzene also extends its influence to high temperatures, but not as significantly as the 3-pentanone.

Fig. 3(a) shows the XRD patterns for the pyrolyzed SiOC samples. All the samples show an amorphous SiO_2 halo centered around 22° [30]. In addition, all the samples exhibit a peak at approximately 44°, corresponding to the (100) plane of turbostratic carbon [30–33]. The 200 vol% conditions for each of the three solvents also display β-SiC peaks at 35.6°, 60°, and 72°, which is not seen for the pure PSO sample. No α-SiC is observed in any of the samples, consistent with previous studies using the same PSO precursor [20,21,34]. The 3-pentanone sample shows the greatest amount of SiC, and the isobutylbenzene shows the least SiC formation for the three solvents. Additionally, the peak at 22° is shifted to ~23.5° for the 200-p sample (as shown by the dashed line in Fig. 3(a)). Likely, the lower content of SiO_2 within the 200-p sample leads to the more prominent (002) peak of the turbostratic carbon at ~26° [21,33] and causes the observed peak shift. A similar shift has been observed for SiOC ceramics after etching out SiO_2 with hydrofluoric acid [20,21,34,35].

The XRD patterns for the samples with 50, 100, and 200 vol% 3-pentanone are shown in Fig. 3(b). The 50-p sample shows diffraction peaks similar to the PSO sample. However, with the addition of 100 vol% or 200 vol% 3-pentanone, the sample shows significant formation of SiC.

The fracture surfaces of the pyrolyzed SiOC samples with 200 vol% solvents have been examined using scanning electron microscopy. All of the fracture surfaces show identical, featureless microstructures despite the differences in phase composition. This is to be expected due to the nanostructure of SiOC, in which the various phases have only single nanometer sizes [19,36–38]. Thus, the SEM images of the fracture surfaces confirm that the microstructure for the SiOC samples remains in the nanometer size range despite the addition of the various solvents.

3.3. Fundamental understanding

The presence of the SiO_2, SiC, and carbon diffraction peaks for the samples after pyrolysis occurs due to the phase separation of SiOC, as well as the carbothermal reduction of SiO_2 into SiC. The main reactions that produce SiO_2, SiC, and C within the ceramics are given by Refs. [37,39]:

$$2SiOC \rightarrow SiO_2(amorphous) + SiC(\beta) + C \quad (2)$$

$$SiO_2(amorphous) + 3C \rightarrow SiC(\beta) + 2CO\uparrow \quad (3)$$

The fundamental reason for the increased SiC formation when the solvents are used can be understood based on the diffusion and penetration of the solvents in-between the PSO chains, which causes increased polymer chain entanglement along with some trapped residual solvent, as illustrated in Fig. 4. 3-pentanone has the smallest molecular volume of the three solvents (3-pentanone: 0.18 nm^3; n-heptane: 0.24 nm^3; isobutylbenzene: 0.26 nm^3), so it would most easily diffuse within the PSO polymer, be trapped during drying, increase the polymer chain entanglement, and thus influence the SiOC phase evolution during pyrolysis. The 3-pentanone molecules can also supply additional carbon and facilitate SiC formation following Eq. (3) due to its complete mixing with the polymer chains/decomposed radical species. Fig. 5 shows the Raman spectroscopic results of the SiOC samples with different types of solvents (Fig. 5(a)) and different amount of 3-pentanone solvent (Fig. 5(b)) after pyrolysis at 1100 °C. The most dominant features of the free carbon are the disorder-induced D band at 1350 cm^{-1} and the ordered graphite G band at 1588 cm^{-1}. The broad G′ band at 2682 cm^{-1} and the weak band at 2934 cm^{-1} can be assigned to a combination of the defect/disordering and graphitic modes (G + D). The Lorentzian curve fitting of the D and G bands can be used to extract the I_D/I_G intensity ratio, which is also shown in Fig. 5. It should be noticed that the complete mixing of the solvents with the PSO precursor is a pre-condition as the I_D/I_G peak ratios from the Raman results in Fig. 5(a) do not correlate with the XRD results in Fig. 3(a). However, the I_D/I_G peak ratios for the samples of different 3-pentanone solvent amounts correlate consistently with the amount of the solvent amount used. On a relative sense, more 3-pentanone leads to more ordered graphitic carbon formation. At the same time, the total amount of carbon and thus the absolute amount of amorphous carbon should also increase and lead to more SiC formation, as shown in Fig. 3(b). For n-heptane and isobutylbenzene, their larger sizes hinder their ability to efficiently penetrate in-between polymer chains or cause polymer chain alignment. Even with more isobutylbenzene presence (Fig. 2(c)), its impact on SiC formation is negligible. It should be understood that the trapped solvent amount on the sample surface must be small, as it is undetectable by FT-IR (Fig. 2). Thus, intimate mixing of the residual solvent with the polymer chains becomes a key factor. Such effect does

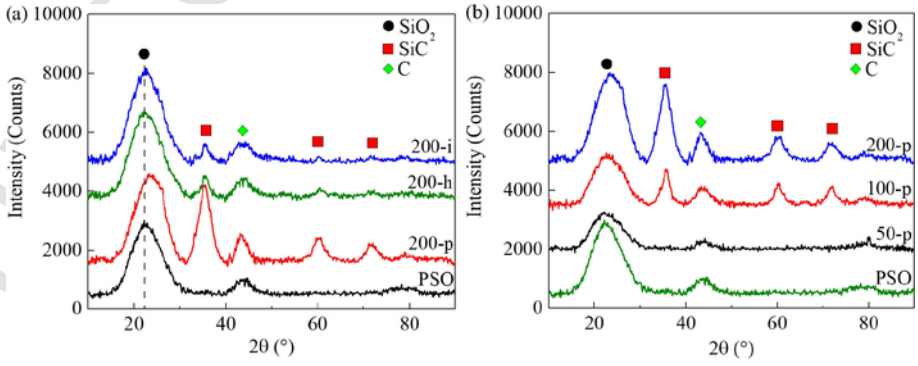

Fig. 3. XRD patterns for the PSO samples with different solvents after pyrolysis at 1300 °C. (**a**) 200 vol% for each solvent, and (**b**) different amounts for 3-pentanone.

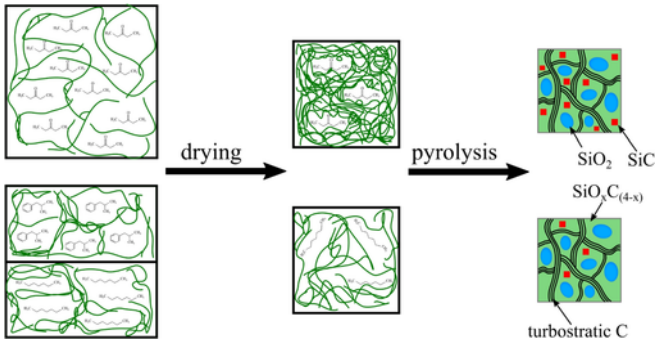

Fig. 4. Solvent size effect on its ability to increase polymer chain entanglement, remain within the polymer after drying, and affect SiC formation.

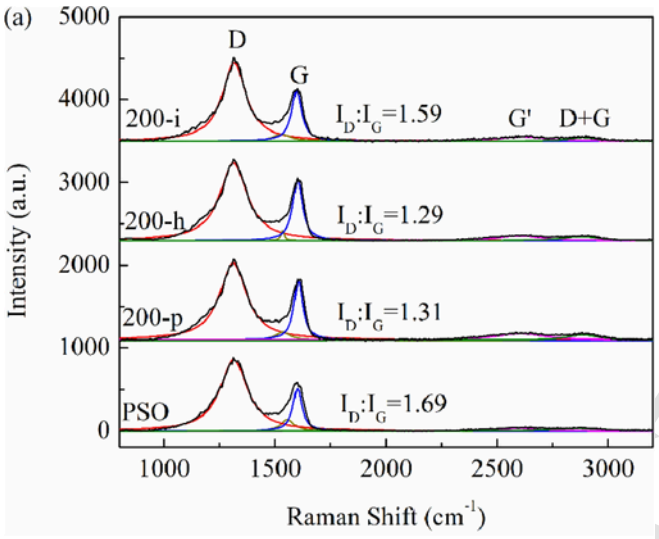

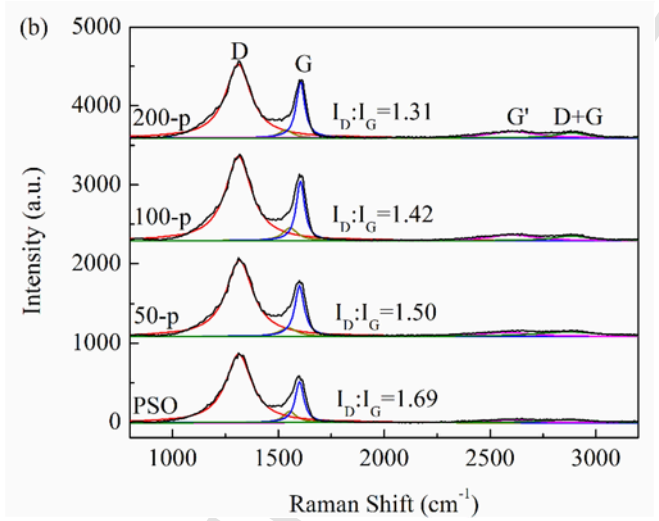

Fig. 5. Raman spectroscopic results of the SiOC samples with different types of solvents **(a)** and different amount of 3-pentanone solvent **(b)** after pyrolysis at 1100 °C.

not directly translate to macroscopic properties as discussed in Section 3.1.

The more dominant influence of 3-pentanone in forming SiC compared to the other two solvents is shown in Fig. 6, which displays the integrated area percentages for SiO_2 (21.6°), SiOC (22.7°), SiC (35.6°, 60°, 72°), and C (26°, 43°) for the PSO and 200 vol% solvent samples. The 200 vol% sample has the highest amount of SiC. It should be noted

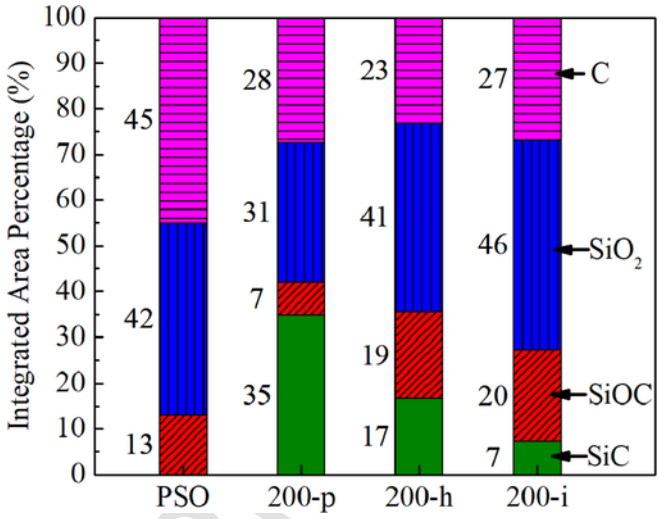

Fig. 6. XRD intensity ratios of SiO_2 (21.6°), SiOC (22.7°), SiC (35.6°, 60°, 72°), and C (26°, 43°) for the PSO and 200 vol% solvent samples after 1300 °C pyrolysis.

that the data in Fig. 6 are not meant as a quantitative measure of the actual phase compositions due to the largely amorphous nature of the SiOC but rather a means to compare the relative phase compositions between the samples. All of the solvent-containing samples contain much less free C compared to the PSO sample. Further, the 200-p sample has the highest SiC content and the lowest SiO_2 and SiOC contents.

4. Conclusions

The crosslinking of polysiloxane-based polymers with different solvents and solvent concentrations has been investigated. Compared to the sample crosslinked with no solvent, most of the solvent-containing samples show a decrease in bulk density and an increase in porosity. The presence of the solvents during crosslinking encourages the formation of nanocrystalline SiC, which is absent in the pure PSO sample. The SiC formation is more prominent when high concentrations of solvents are present during crosslinking. Additionally, the SiC formation is dependent on the size of the solvent molecules, with smaller solvent molecules leading to more SiC formation. Based on the concentration and molecular size, the SiC formation can be linked to the increased polymer chain entanglement and retention of the solvent in the crosslinked polymer after drying.

Conflicts of interest

The authors declare that they have no conflict of interest.

Acknowledgements

We acknowledge the financial support from National Science Foundation under grant number CMMI-1634325.

References

[1] P. Colombo, G. Mera, R. Riedel, G.D. Soraru, Polymer-derived ceramics: 40 years of research and innovation in advanced ceramics, J. Am. Ceram. Soc. 93 (2010) 1805–1837.
[2] K. Lu, D. Erb, M. Liu, Thermal stability and electrical conductivity of carbon-enriched silicon oxycarbide, J. Mater. Chem. C 4 (2016) 1829–1837.
[3] K. Lu, D. Erb, M.Y. Liu, Phase transformation, oxidation stability, and electrical conductivity of tio2-polysiloxane derived ceramics, J. Mater. Sci. 51 (2016) 10166–10177.
[4] Y. Juttke, H. Richter, I. Voigt, R.M. Prasad, M.S. Bazarjani, A. Gurlo, R. Riedel, Polymer derived ceramic membranes for gas separation, Chem. Eng. Trans. 32 (2013) 1891–1896.
[5] P. Dibandjo, M. Graczyk-Zajac, R. Riedel, V.S. Pradeep, G.D. Soraru, Lithium insertion into dense and porous carbon-rich polymer-derived sioc ceramics, J. Eur. Ceram. Soc. 32 (2012) 2495–2503.

[6] V.S. Pradeep, D.G. Ayana, M. Graczyk-Zajac, G.D. Soraru, R. Riedel, High rate capability of sioc ceramic aerogels with tailored porosity as anode materials for li-ion batteries, Electrochim. Acta 157 (2015) 41–45.
[7] J.D. Torrey, R.K. Bordia, Mechanical properties of polymer-derived ceramic composite coatings on steel, J. Eur. Ceram. Soc. 28 (2008) 253–257.
[8] T. Rouxel, G. Massouras, G.D. Soraru, High temperature behavior of a gel-derived sioc glass: elasticity and viscosity, J. Sol. Gel Sci. Technol. 14 (1999) 87–94.
[9] S. Smitha, P. Shajesh, P.R. Aravind, S.R. Kumar, P.K. Pillai, K.G.K. Warrier, Effect of aging time and concentration of aging solution on the porosity characteristics of subcritically dried silica aerogels, Microporous Mesoporous Mater. 91 (2006) 286–292.
[10] C. Liu, X.Y. Meng, X.H. Zhang, C.Q. Hong, J.C. Han, W.B. Han, B.S. Xu, S. Dong, S.Y. Du, High temperature structure evolution of macroporous sioc ceramics prepared by a sol-gel method, Ceram. Int. 41 (2015) 11091–11096.
[11] C.L. Liu, H.X.Z. Chen, S. Komarneni, C.G. Pantano, High surface area sic/silicon oxycarbide glasses prepared from phenyltrimethoxysilane-tetramethoxysilane gels, J. Porous Mater. 2 (1995) 245–252.
[12] P.V.W. Sasikumar, E. Zera, M. Graczyk-Zajac, R. Riedel, G.D. Soraru, Structural design of polymer-derived sioc ceramic aerogels for high-rate li ion storage applications, J. Am. Ceram. Soc. 99 (2016) 2977–2983.
[13] A. Tamayo, J. Rubio, F. Rubio, J.L. Oteo, R. Riedel, Texture and micro-nanostructure of porous silicon oxycarbide glasses prepared from hybrid materials aged in different solvents, J. Eur. Ceram. Soc. 31 (2011) 1791–1801.
[14] A. Tamayo, F. Rubio, J. Rubio, J.L. Oteo, Surface and structural modification of nanostructured mesoporous silicon oxycarbide glasses obtained from preceramic hybrids aged in nh4oh, J. Am. Ceram. Soc. 96 (2013) 323–330.
[15] A. Tamayo, J. Rubio, Structure modification by solvent addition into teos/pdms hybrid materials, J. Non-Cryst. Solids 356 (2010) 1742–1748.
[16] Y. Blum, G.D. Soraru, A.P. Ramaswamy, D. Hui, S.M. Carturan, Controlled mesoporosity in sioc via chemically bonded polymeric “spacers”, J. Am. Ceram. Soc. 96 (2013) 2785–2792.
[17] J.L. Wan, M.J. Gasch, A.K. Mukherjee, In situ densification behavior in the pyrolysis consolidation of amorphous si-n-c bulk ceramics from polymer precursors, J. Am. Ceram. Soc. 84 (2001) 2165–2169.
[18] N. Janakiraman, F. Aldinger, Fabrication and characterization of fully dense si-c-n ceramics from a poly (ureamethylvinyl) silazane precursor, J. Eur. Ceram. Soc. 29 (2009) 163–173.
[19] S. Martinez-Crespiera, E. Ionescu, H.J. Kleebe, R. Riedel, Pressureless synthesis of fully dense and crack-free sioc bulk ceramics via photo-crosslinking and pyrolysis of a polysiloxane, J. Eur. Ceram. Soc. 31 (2011) 913–919.
[20] D. Erb, K. Lu, Additive and pyrolysis atmosphere effects on polysiloxane-derived porous sioc ceramics, J. Eur. Ceram. Soc. 37 (2017) 4547–4557.
[21] J.K. Li, K. Lu, Highly porous sioc bulk ceramics with water vapor assisted pyrolysis, J. Am. Ceram. Soc. 98 (2015) 2357–2365.
[22] P.R. Aravind, G.D. Soraru, Porous silicon oxycarbide glasses from hybrid ambigels, Microporous Mesoporous Mater. 142 (2011) 511–517.
[23] J.R. Rumble, Crc Handbook of Chemistry and Physics, 98th ed., CRC Press/Taylor & Francis, Boca Raton, FL, 2005.
[24] M. Halim, C. Hudaya, A.Y. Kim, J.K. Lee, Phenyl-rich silicone oil as a precursor for sioc anode materials for long-cycle and high-rate lithium ion batteries, J. Mater. Chem. A 4 (2016) 2651–2656.
[25] G. Camino, S.M. Lomakin, M. Lageard, Thermal polydimethylsiloxane degradation. Part 2. The degradation mechanisms, Polymer 43 (2002) 2011–2015.
[26] D. Hourlier, S. Venkatachalam, M.R. Ammar, Y. Blum, Pyrolytic conversion of organopolysiloxanes, J. Anal. Appl. Pyrolysis 123 (2017) 296–306.
[27] R. Ma, K. Lu, D. Erb, Effect of solvent in preparation of SiOC bulk ceramics, Mater. Chem. Phys. 218 (2018) 140–146.
[28] A. Nyczyk-Malinowska, M. Wojcik-Bania, T. Gumula, M. Hasik, M. Cypryk, Z. Olejniczak, New precursors to sico ceramics derived from linear poly(vinylsiloxanes) of regular chain composition, J. Eur. Ceram. Soc. 34 (2014) 889–902.
[29] M. Hasik, M. Wojcik-Bania, A. Nyczyk, T. Gumula, Polysiloxane-poss systems as precursors to sico ceramics, React. Funct. Polym. 73 (2013) 779–788.
[30] R. Peña-Alonso, G.D. Sorarù, R. Raj, Preparation of ultrathin-walled carbon-based nanoporous structures by etching pseudo-amorphous silicon oxycarbide ceramics, J. Am. Ceram. Soc. 89 (2006) 2473–2480.
[31] A.M. Wilson, G. Zank, K. Eguchi, W. Xing, B. Yates, J.R. Dahn, Pore creation in silicon oxycarbides by rinsing in dilute hydrofluoric acid, Chem. Mater. 9 (1997) 2139–2144.
[32] R. Pena-Alonso, G. Mariotto, C. Gervais, F. Babonneau, G.D. Soraru, New insights on the high-temperature nanostructure evolution of sioc and b-doped siboc polymer-derived glasses, Chem. Mater. 19 (2007) 5694–5702.
[33] Z.Q. Li, C.J. Lu, Z.P. Xia, Y. Zhou, Z. Luo, X-ray diffraction patterns of graphite and turbostratic carbon, Carbon 45 (2007) 1686–1695.
[34] J.K. Li, K. Lu, T.S. Lin, F.Y. Shen, Preparation of micro-/mesoporous sioc bulk ceramics, J. Am. Ceram. Soc. 98 (2015) 1753–1761.
[35] P. Dibandjo, S. Dire, F. Babonneau, G.D. Soraru, New insights into the nanostructure of high-c sioc glasses obtained via polymer pyrolysis, Glass Technol.: Eur. J. Glass Sci. Technol., Part A 49 (2008) 175–178.
[36] A. Saha, R. Raj, D.L. Williamson, A model for the nanodomains in polymer-derived sico, J. Am. Ceram. Soc. 89 (2006) 2188–2195.
[37] H.J. Kleebe, C. Turquat, G.D. Soraru, Phase separation in an sico glass studied by transmission electron microscopy and electron energy-loss spectroscopy, J. Am. Ceram. Soc. 84 (2001) 1073–1080.
[38] Y.D. Blum, D.B. MacQueen, H.-J. Kleebe, Synthesis and characterization of carbon-enriched silicon oxycarbides, J. Eur. Ceram. Soc. 25 (2005) 143–149.
[39] A. Saha, R. Raj, Crystallization maps for sico amorphous ceramics, J. Am. Ceram. Soc. 90 (2007) 578–583.